Center-to-Edge Denoising Diffusion Probabilistic Models with Cross-domain Attention for Undersampled MRI Reconstruction

Jianfeng Zhao[1] and Shuo Li[2,3(✉)]

[1] School of Biomedical Engineering, Western University, London, ON, Canada
[2] School of Biomedical Engineering, Case Western Reserve University, Cleveland, OH, USA
[3] School of Computer and Data Sciences, Case Western Reserve University, Cleveland, OH, USA slishuo@gmail.com

Abstract. Integrating dual-domain (i.e. frequency domain and spatial domain) information for magnetic resonance imaging (MRI) reconstruction from undersampled measurements greatly improves imaging efficiency. However, it is still a challenging task using the denoising diffusion probabilistic models (DDPM)-based method, due to the lack of an effective fusion module to integrate dual-domain information, and there is no work exploring the effect that comes from denoising diffusion strategy on dual-domain. In this study, we propose a novel center-to-edge DDPM (C2E-DDPM) for fully-sampled MRI reconstruction from undersampled measurements (i.e. undersampled k-space and undersampled MR image) by improving the learning ability in the frequency domain and cross-domain information attention. Different from previous work, C2E-DDPM provides a C2E denoising diffusion strategy for facilitating frequency domain learning and designs an attention-guided cross-domain junction for integrating dual-domain information. Experiments indicated that our proposed C2E-DDPM achieves state-of-the-art performances in the dataset fastMRI (i.e. The scores of PSNR/SSIM of 33.26/88.43 for 4× acceleration and 31.67/81.94 for 8× acceleration).

Keywords: Denoising diffusion probabilistic models · Dual-domain · Undersampled · MRI Reconstruction.

1 Introduction

Integrating dual-domain information for MRI reconstruction is still challenging and of great significance for clinical examination. Magnetic resonance imaging (MRI), as a non-invasive imaging technique, is extensively utilized. However, a drawback of MRI is that it causes discomfort for individuals due to the need to lie still for extended periods in a cramped and confined space. Thus, with the aim of reducing MR scanning time, reconstructing MR images from undersampled measurements has a long and extensive history of research [18]. According to the source image, the existing works of MRI reconstruction can be divided into two

parts: single domain based (i.e. single frequency domain [21] or single spatial domain [2,3]) and cascade dual domain based [20]. However, the single domain-based method ignores the complementary prior information [22] and the cascade dual domain-based method brings the accumulation error [6].

Although denoising diffusion probabilistic models (DDPM) [7] show superior performance in reconstruction tasks, no work explores the effect of denoising diffusion strategy on dual-domain medical images. DDPM has shown great power in various synthesis tasks (e.g. image [4,13], audio [11], in-painting [12], and super-resolution [16]). And some works have attempted to deploy the DDPM-based method for MRI reconstruction from undersampled measurements [15,21]. However, few work explores the effect of denoising diffusion strategy on the frequency domain and spatial domain. As shown in Fig.1.(a), existing works deploy traditional denoising diffusion strategy [7] using global Gaussian noise to both the frequency domain and spatial domain. For spatial domain, it has the advantage of keeping the context anatomy features in the sampling steps because it follows the spatial domain imaging characteristics. But for frequency domain, using global Gaussian noise brings the risk of extra sampling steps. Besides, frequency domain information is sensitive to noise (small reconstruction errors in the frequency domain cause unpredictable influence in the spatial domain) [6]. Thus, designing a tailored denoising diffusion strategy for frequence domain learning following frequency imaging characteristics has great potential to improve learning ability and speed up DDPM.

Designing a center-to-edge (C2E) denoising diffusion strategy following the frequency characteristics for facilitating frequency domain processing. As shown in Fig.1(b), the frequency domain shows incomprehensible information to human vision [6] but there is no doubt that the signal is divergent from the center-to-edge [14]. Specifically, the center stores high signal energy to represent the low-frequency signal such as the global contour feature, and the edge stores low signal energy to represent the high-frequency signal such as the detailed texture feature. Recently, Bansal et al. [1] first indicated that the behavior of denoising diffusion in DDPM exhibits a limited dependence on the choice of Gaussian noise, and in fact, the DDPM can be constructed by using a different choice of noise. Inspired by these works, the hypothesis of this work is to design a C2E denoising diffusion strategy following the frequency characteristics of C2E for facilitating frequency domain processing, which is shown in first stage of Fig.1(c).

In this paper, we propose a novel center-to-edge denoising diffusion probabilistic models (C2E-DDPM) for fully-sampled MRI reconstruction from undersampled measurements (i.e. undersampled k-space and undersampled MR image) by improving the learning ability in the frequency domain and cross-domain information attention. Our method differs from previous works [2,15,21,24] in two key aspects: (1) the diffusion and sampling process is defined in dual-domain with C2E denoising diffusion strategy rather than traditional denoising diffusion operation in DDPM [7]; (2) using parallel optimization between frequency domain (i.e. k-space) and spatial domain (i.e. MR image) rather than using single domain information or simply concatenation. The main contributions can be summarized

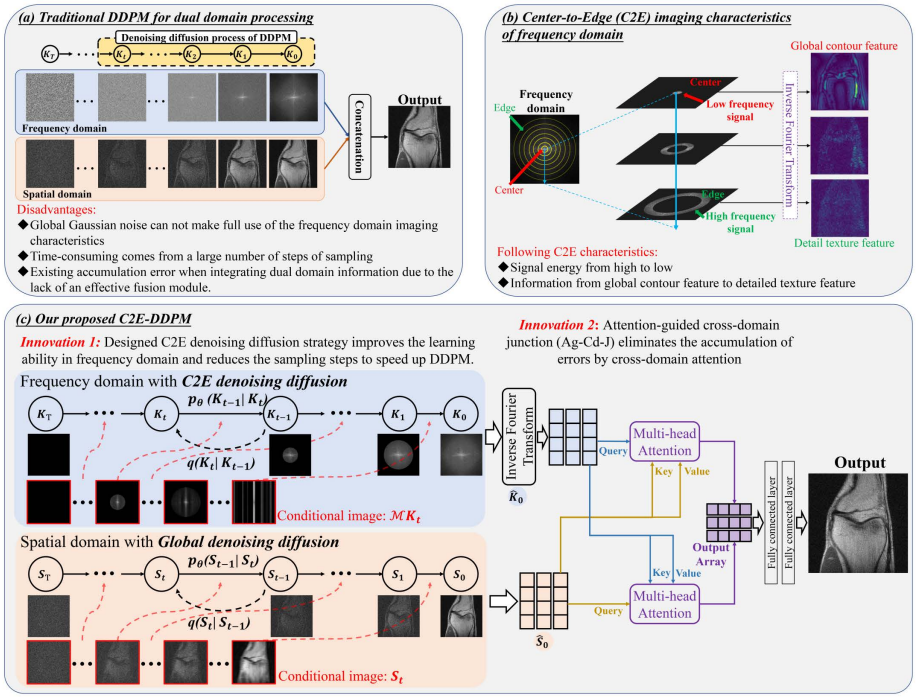

Fig. 1. Advantages of our proposed C2E-DDPM. From (a) to (c), they are disadvantages of traditional DDPM for dual domain processing, center-to-edge imaging characteristics of frequency domain, and overview of our proposed C2E-DDPM, respectively.

as: (1) We propose a novel C2E denoising diffusion strategy according to the frequency domain characteristics, which facilitates DDPM training and reduces the sampling steps for the dual-domain information denoising diffusion process. (2) To effectively integrate dual-domain information, an attention-guided cross-domain junction (Ag-Cd-J) is proposed to eliminate the accumulation of error between dual domains. (3) Experiments on accelerated MRI reconstruction show C2E-DDPM outperforms State-of-The-Art (SoTA) methods.

2 Method

The C2E-DDPM is implemented based on DDPM [7] for undersampled MRI reconstruction. To ensure the generated MR images follow data consistency with the undersampled measurements, extra conditional guidance is utilized on the basis of DDPM [7]. In addition, a novel C2E denoising diffusion strategy is proposed to facilitate the denoising diffusion process of DDPM by taking into account the frequency domain characteristics. Finally, the Ag-Cd-J is designed for dual-domain information integration. The algorithm process of C2E-DDPM

is organized as follows: preliminary knowledge of DDPM in Sect.2; conditional guidance by undersampled measurements in Sect.2.1; C2E denoising diffusion strategy in Sect.2.2; Ag-Cd-J for dual domain integration in Sect.2.3.

Preliminaries: DDPM [7], as an unconditional generative method, denotes the form of $p_\theta(\mathbf{x}_0) := \int p_\theta(\mathbf{x}_{0:T})\mathrm{d}\mathbf{x}_{1:T}$, where $\mathbf{x}_1, ..., \mathbf{x}_T$ represent latents with the same dimensionality as the data $\mathbf{x}_0 \sim q(\mathbf{x}_0)$. It mainly contains the forward diffusion process and the reverse process of denoising. For reverse process of denoising (i.e. the joint distribution $p_\theta(\mathbf{x}_{0:T})$), it can be defined as a Markov chain with learned Gaussian transitions starting from $p(\mathbf{x}_T) = \mathcal{N}(\mathbf{x}_T; \mathbf{0}, \mathbf{I})$:

$$p_\theta(\mathbf{x}_{t-1}|\mathbf{x}_t) := \mathcal{N}(\mathbf{x}_{t-1}; \mu_\theta(\mathbf{x}_t, t), \sigma_t^2\mathbf{I}), \quad p_\theta(\mathbf{x}_{0:T}) := p(\mathbf{x}_T)\prod_{t=1}^{T} p_\theta(\mathbf{x}_{t-1}|\mathbf{x}_t) \quad (1)$$

Where μ_θ is the estimated mean yielded by a neural network parameterized by θ. For the forward diffusion process (i.e. the approximate posterior $q(\mathbf{x}_{1:T}|\mathbf{x}_0)$), it is a Markov Chain that involves the gradual addition of Gaussian noise to convert the data distribution to the noise distribution according to the variance schedule β_1, ..., β_T:

$$q(\mathbf{x}_t|\mathbf{x}_{t-1}) := \mathcal{N}(\mathbf{x}_t; \sqrt{1-\beta_t}\mathbf{x}_{t-1}, \beta_t\mathbf{I}), \quad q(\mathbf{x}_t|\mathbf{x}_0) = \mathcal{N}(\mathbf{x}_t; \sqrt{\bar{\alpha}_t}\mathbf{x}_0, (1-\bar{\alpha}_t)\mathbf{I}) \quad (2)$$

where $\alpha_t := 1 - \beta_t$, $\bar{\alpha}_t := \prod_{s=1}^{t} \alpha_s$, and $\sigma_t^2 = \frac{1-\bar{\alpha}_{t-1}}{1-\bar{\alpha}_t}\beta_t$.

2.1 Conditional DDPM by undersampled measurements

In the traditional DDPM, the unconditional generation $\mathbf{x}_{t-1}$ at each step is obtained by subtracting the predicted noise from the previous $\mathbf{x}_t$, which as defined in [7]:

$$\mathbf{x}_{t-1} = \frac{1}{\sqrt{\alpha_t}}(\mathbf{x}_t - \frac{1-\alpha_t}{\sqrt{1-\bar{\alpha}_t}}\epsilon_\theta(\mathbf{x}_t, t)) + \sigma_t\mathbf{z}, \quad \mathbf{z} \sim \mathcal{N}(0, \mathbf{I}) \quad (3)$$

Where ϵ_θ is defined as a function approximator intended to predict ϵ from $\mathbf{x}_t$. To perform the conditional generation in C2E-DDPM, the generation $\mathbf{x}_{t-1}$ at each step is on the basis of $\hat{\mathbf{x}}_t$, which mixes undersampled measurements $\mathbf{X}_{C,t}$ with $\mathbf{x}_t$.Thus, the $\mathbf{x}_{t-1}$ here can be defined as:

$$\mathbf{x}_{t-1} = \frac{1}{\sqrt{\alpha_t}}(\mathbf{x}_t - \frac{1-\alpha_t}{\sqrt{1-\bar{\alpha}_t}}\epsilon_\theta(\hat{\mathbf{x}}_t, t)) + \sigma_t\mathbf{z}, \quad \mathbf{z} \sim \mathcal{N}(0, \mathbf{I}) \quad (4)$$

In this work, the conditional matrix of undersampled measurements $\mathbf{X}_C \in \{\mathcal{M}\mathbf{K}_t, \mathbf{S}_t\}$ has two types according to the specific domain (i.e. undersampled k-space matrix $\mathcal{M}\mathbf{K}_t$ in the frequency domain and undersampled MRI matrix $\mathbf{S}_t$ in the spatial domain). So, the $\hat{\mathbf{x}}_t$ also has two types of calculation corresponding to the frequency domain $\hat{\mathbf{x}}_{t,k}$ and spatial domain $\hat{\mathbf{x}}_{t,s}$. For frequency domain:

$$\hat{\mathbf{x}}_{t,k} = (1-\mathcal{M})\mathbf{x}_{t,k} + \mathcal{M}\mathbf{K}_t, \quad \mathcal{M}\mathbf{K}_t = \mathcal{M}\mathbf{K}_0 + \mathcal{F}(\mathcal{N}(0, (1-\bar{\alpha}_t)\mathbf{I})) \quad (5)$$

where $\mathcal{M}$ presents the undersampled mask image, $\mathcal{F}$ presents the Fourier Transform, $\mathbf{K}_0$ presents the fully sampled k-space, and $\mathcal{N}(0,(1-\bar{\alpha}_t)\mathbf{I})$ presents a zero-mean noise for the simulation of diffusion condition in each step. For spatial domain:

$$\hat{\mathbf{x}}_{t,s} = \mathbf{x}_{t,s} + \mathbf{S}_t, \quad \mathbf{S}_t = \mathbf{S}_0 + \mathcal{N}(0,(1-\bar{\alpha}_t)\mathbf{I}) \tag{6}$$

where $\mathbf{S}_0$ presents the fully sampled MR image.

2.2 C2E denoising diffusion strategy

As shown in Fig.1, a novel C2E denoising diffusion strategy is proposed according to the frequency domain characteristics. Specifically, for **spatial domain**, to ensure the global context feature extraction in the whole MR image when using U-Net [17] to achieve the diffusion process, it deploys the global denoising diffusion strategy proposed in traditional DDPM [7]. For **frequency domain**, according to the divergence from the C2E characteristics in k-space, the frequency domain follows the low-to-high frequency denoising diffusion strategy by using a circular Gaussian mask to remove pixels. First, we define a discretized 2D Gaussian array of variance η, in which the spatial resolution is consistent with the size of k-space $n \times n$. Next, normalize the 2D Gaussian array so that the peak of the array equals 1. And then, the circular Gaussian mask is achieved by subtracting the result from 1 (i.e. the center of the mask equals 0). Finally, the input fully sampled k-space $\mathbf{K}_0$ and conditional matrix $\mathcal{M}\mathbf{K}_t$ gradually masked for T steps by using the circular Gaussian mask image $\mathbf{z}_{\eta_i}$ with increasing η_i [1]. According to the work [1], the k-space image and conditional matrix in step t that $\mathbf{K}_t$ and $\mathcal{M}\mathbf{K}_t$ can be calculated as:

$$\mathbf{K}_t = \mathbf{K}_0 \otimes \prod_{i=1}^{t} \mathbf{z}_{\eta_i}, \quad \mathcal{M}\mathbf{K}_t = \mathcal{M}\mathbf{K}_0 \otimes \prod_{i=1}^{t} \mathbf{z}_{\eta_i} \tag{7}$$

where $\otimes$ presents entry-wise multiplication.

2.3 Ag-Cd-J for dual domain integration

As shown in Fig.1, after dual domain prediction of fully sampled k-space $\hat{\mathbf{K}}_0$ and fully sampled MR image $\hat{\mathbf{S}}_0$, an Ag-Cd-J is designed for dual domain integration. The cross-domain junction basically relies on the multi-head attention layer proposed in work [19]. The work [19] utilized the multi-head attention layer to improve the context feature extraction in a single input image. And the work [8] proved the effectiveness of the multi-head attention layer for various inputs. Inspired by these two works, our Ag-Cd-J designs a parallel attention path for dual-domain interaction with cross-domain attention. Take the calculation of the cross-attention in the spatial path as an example. After the Inverse Fourier Transform of $\hat{\mathbf{K}}_0$, the yielded matrix is fed into attention layer from the key and value paths while $\hat{\mathbf{S}}_0$ is fed into attention from query path. The cross-attention in the frequency path utilizes a similar calculation except for feeding the Inverse Fourier Transform of $\hat{\mathbf{K}}_0$ from the query path and feeding $\hat{\mathbf{S}}_0$ from key and

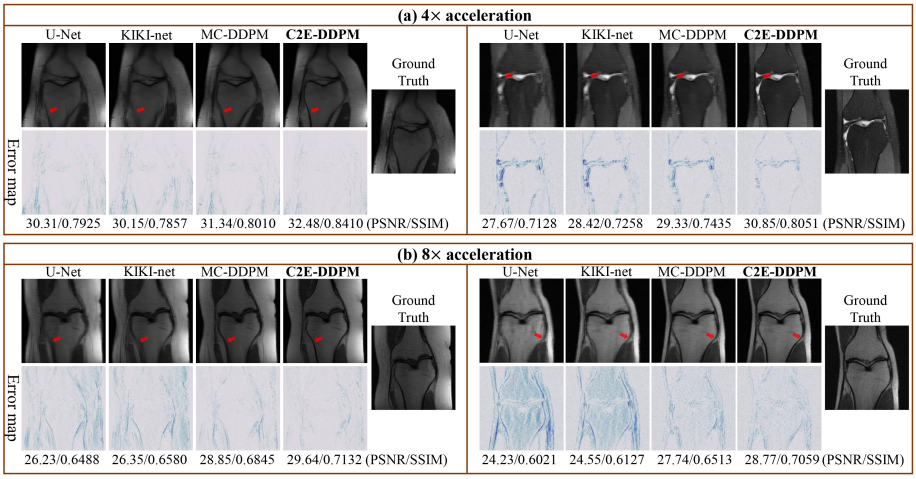

Fig. 2. Visualized comparison of C2E-DDPM with other methods. (a) is reconstruction results of 4× acceleration and (b) is reconstruction results of 8× acceleration. Error map is obtained by making a difference between ground truth and reconstructed image.

value paths. The calculation of the multi-head attention layer in Ag-Cd-J can be defined as:

$$Attention(\mathrm{Q},\mathrm{K},\mathrm{V}) = softmax(\frac{\mathrm{Q}\mathrm{K}^{\mathrm{T}}}{\sqrt{d_k}})\mathrm{V} \tag{8}$$

where $\mathrm{Q} = \mathrm{W}_{\mathrm{Q}} \cdot \hat{\mathbf{S}}_0$, $\mathrm{K} = \mathrm{W}_{\mathrm{K}} \cdot \hat{\mathbf{K}}_0$, and $\mathrm{V} = \mathrm{W}_{\mathrm{V}} \cdot \hat{\mathbf{K}}_0$, and W_{Q}, W_{K}, and W_{V} are learnable projection matrices [8,19]. Finally, to eliminate the accumulation of errors between dual domains via dual domain integration, the $\mathcal{L}_2$ loss function is deployed to optimize the Ag-Cd-J. It captures the complementary information and establishes coherent constraints between dual domains.

3 Experiment and Results

Dataset. The effectiveness of C2E-DDPM is validated in a large publicly available[4] single-coil knee MR dataset fastMRI [23], which totally contains 1172 subjects. In our experiment, 938 subjects are used for training and 234 subjects are used for evaluation. The size of both k-space date and spatial domain MR image data are 320 × 320 pixels. The undersampled masks image $\mathcal{M}$ are yielded by using the mask function provided in fastMRI challenge [23] with 4× and 8× accelerations.

Implementation Details. The noise schedule follows improved-DDPM [13], and the U-Net [17] was used for the denoising model with 200 sampling steps in

[4] https://fastmri.org.

Table 1. The quantitative evaluation of the comparison between C2E-DDPM and other methods. The criteria of PSNR & SSIM evaluated the performance of our C2E-DDPM and other three other methods.

	4× Acceleration			
	U-Net	KIKI-net	MC-DDPM	**C2E-DDPM**
PSNR	30.81	31.04	31.68	**33.26**
SSIM	79.45	81.80	83.88	**88.43**
	8× Acceleration			
PSNR	28.15	29.34	29.77	**31.67**
SSIM	66.94	74.88	73.39	**81.94**

both the k-space domain and spatial domain. Inspired by Vaswani et al. [19], the scaling factor d_k was set to 64 in equation 8. The denoising process was trained with an $\mathcal{L}_1$ loss function, and the Ag-Cd-J was trained with an $\mathcal{L}_2$ loss function using a learning rate of 0.0001 and the Adam optimizer [9]. The C2E-DDPM was implemented on an Ubuntu 20.04 platform using Pytorch and the CUDA library, and was run on an RTX 3090Ti GPU.

Quantitative and Visual Evaluation. To verify the performance of C2E-DDPM, we campared it with three methods: (1) a baseline model U-Net [17] in [10]; (2) a SoTA method KIKI-net [5], which deploys CNNs to integrate the k-space domain and spatial domain for reconstruction; (3) a DDPM-based method measurement-conditioned denoising diffusion probabilistic model (MC-DDPM) [21] for knee MRI reconstruction. The peak signal-to-noise ratio (PSNR) and structural similarity index (SSIM) were used for evaluation criteria. The visualized results with 4× and 8× acceleration are shown in Fig.2. The comparison shows that many detailed structures are lost in three compared methods (i.e. where the red arrow points), but can be reconstructed by C2E-DDPM. The quantitative results with 4× and 8× acceleration are shown in Table 1. Our C2E-DDPM achieved the highest scores of PSNR and SSIM. Compared to the MC-DDPM [21], our method outperforms by 1.58/4.55 for 4× acceleration and 1.9/7.95 for 8× acceleration in PSNR/SSIM. All these results proved the superiority of our proposed C2E-DDPM.

Table 2. The quantitative evaluation of the ablation study. The criteria of PSNR & SSIM evaluated the performance. Both the C2E denoising diffusion strategy and Ag-Cd-J contribute to undersampled MRI reconstruction.

	4× Acceleration			8× Acceleration		
	No C2E	No Ag-Cd-J	**C2E-DDPM**	No C2E	No Ag-Cd-J	**C2E-DDPM**
PSNR	32.18	32.30	**33.26**	30.14	30.31	**31.67**
SSIM	85.76	85.73	**88.43**	76.58	76.78	**81.94**

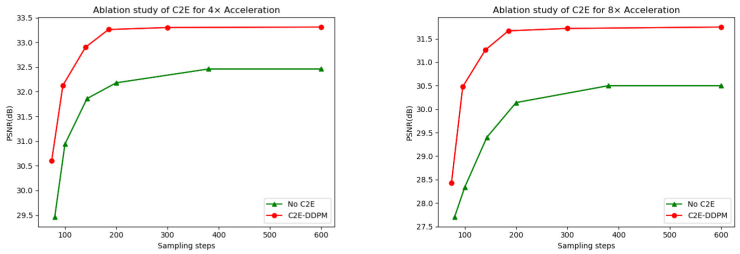

Fig. 3. Ablation study of C2E for MRI reconstruction under different sampling steps. The left is 4× acceleration and the right is 8× acceleration.

Ablation study. To prove the contributions of the C2E denoising diffusion strategy and the cross-domain attention module Ag-Cd-J, we conducted the following two experimental comparisons: (1) For the C2E denoising diffusion strategy, we removed the C2E frequency denoising diffusion strategy in the frequency domain and used the global denoising diffusion strategy in DDPM [7] in both frequency domain and spatial domain, which is named No C2E. (2) For Ag-Cd-J, we replaced Ag-Cd-J with the operation of concatenation to integrate dual-domain, and used a two-channel convolutional layer followed by the fully connected layer for the final integration, which we named No Ag-Cd-J. The quantitative results are shown in Table 2. For both 4× and 8× acceleration reconstruction, both PSNR and SSIM values decreased when we removed either C2E or Ag-Cd-J. In the 8× acceleration reconstruction, the values of PSNR and SSIM decreased the most when removed C2E (i.e., PSNR decreased by 1.53 and SSIM decreased by 5.36). These results demonstrate that both the C2E denoising diffusion strategy and Ag-Cd-J contribute to the undersampled MRI reconstruction.

Moreover, to verify the effect of C2E denoising diffusion strategy on the learning ability and sampling steps of DDPM, Fig.3 shows the performance of No C2E and C2E-DDPM under different sampling steps. For 4× and 8× acceleration MRI reconstruction, compared to the No C2E method, C2E-DDPM achieves higher PSNR values in fewer sampling steps. Specifically, the C2E-DDPM appears to converge when around 200 steps, while No C2E converges at around 400 steps. That means C2E denoising diffusion strategy reduces the sampling steps of DDPM by half.

4 Conclusion

In this paper, we propose a novel approach called C2E-DDPM with cross-domain attention for fully-sampled MRI reconstruction from undersampled measurements. The novel C2E denoising diffusion strategy is designed based on the frequency characteristics of center to edge, which enhances the learning ability in the frequency domain and accelerates DDPM by reducing the required number of sampling steps. This strategy provides an effective way for the DDPM-based

method to process frequency domain information. The Ag-Cd-J module eliminates the error accumulation between dual domains by utilizing the multi-head attention layer to capture complementary information and establish coherent constraints between dual domains. The experimental results indicate the superiority of C2E-DDPM for knee MRI reconstruction, indicating its potential to assist clinical decision-making. Future work includes exploring the contribution of the C2E strategy to the single domain using different MRI datasets and improving the inference speed of C2E-DDPM.

Disclosure of Interests. The authors have no competing interests to declare that are relevant to the content of this article.

References

1. Bansal, A., Borgnia, E., Chu, H.M., Li, J., Kazemi, H., Huang, F., Goldblum, M., Geiping, J., Goldstein, T.: Cold diffusion: Inverting arbitrary image transforms without noise. Advances in Neural Information Processing Systems **36** (2024)
2. Chung, H., Ye, J.C.: Score-based diffusion models for accelerated mri. Medical Image Analysis **80**, 102479 (2022)
3. Deora, P., Vasudeva, B., Bhattacharya, S., Pradhan, P.M.: Structure preserving compressive sensing mri reconstruction using generative adversarial networks. In: Proceedings of the IEEE/CVF Conference on Computer Vision and Pattern Recognition Workshops. pp. 522–523 (2020)
4. Dhariwal, P., Nichol, A.: Diffusion models beat gans on image synthesis. Advances in Neural Information Processing Systems **34**, 8780–8794 (2021)
5. Eo, T., Jun, Y., Kim, T., Jang, J., Lee, H.J., Hwang, D.: Kiki-net: cross-domain convolutional neural networks for reconstructing undersampled magnetic resonance images. Magnetic resonance in medicine **80**(5), 2188–2201 (2018)
6. Ge, R., He, Y., Xia, C., Sun, H., Zhang, Y., Hu, D., Chen, S., Chen, Y., Li, S., Zhang, D.: Ddpnet: A novel dual-domain parallel network for low-dose ct reconstruction. In: Medical Image Computing and Computer Assisted Intervention–MICCAI 2022: 25th International Conference, Singapore, September 18–22, 2022, Proceedings, Part VI. pp. 748–757. Springer (2022)
7. Ho, J., Jain, A., Abbeel, P.: Denoising diffusion probabilistic models. Advances in Neural Information Processing Systems **33**, 6840–6851 (2020)
8. Jaegle, A., Gimeno, F., Brock, A., Vinyals, O., Zisserman, A., Carreira, J.: Perceiver: General perception with iterative attention. In: International conference on machine learning. pp. 4651–4664. PMLR (2021)
9. Kingma, D.P., Ba, J.: Adam: A method for stochastic optimization. arXiv preprint arXiv:1412.6980 (2014)
10. Knoll, F., Zbontar, J., Sriram, A., Muckley, M.J., Bruno, M., Defazio, A., Parente, M., Geras, K.J., Katsnelson, J., Chandarana, H., et al.: fastmri: A publicly available raw k-space and dicom dataset of knee images for accelerated mr image reconstruction using machine learning. Radiology: Artificial Intelligence **2**(1), e190007 (2020)
11. Kong, Z., Ping, W., Huang, J., Zhao, K., Catanzaro, B.: Diffwave: A versatile diffusion model for audio synthesis. arXiv preprint arXiv:2009.09761 (2020)

12. Lugmayr, A., Danelljan, M., Romero, A., Yu, F., Timofte, R., Van Gool, L.: Repaint: Inpainting using denoising diffusion probabilistic models. In: Proceedings of the IEEE/CVF Conference on Computer Vision and Pattern Recognition. pp. 11461–11471 (2022)
13. Nichol, A.Q., Dhariwal, P.: Improved denoising diffusion probabilistic models. In: International Conference on Machine Learning. pp. 8162–8171. PMLR (2021)
14. Paschal, C.B., Morris, H.D.: K-space in the clinic. Journal of Magnetic Resonance Imaging: An Official Journal of the International Society for Magnetic Resonance in Medicine **19**(2), 145–159 (2004)
15. Peng, C., Guo, P., Zhou, S.K., Patel, V.M., Chellappa, R.: Towards performant and reliable undersampled mr reconstruction via diffusion model sampling. In: Medical Image Computing and Computer Assisted Intervention–MICCAI 2022: 25th International Conference, Singapore, September 18–22, 2022, Proceedings, Part VI. pp. 623–633. Springer (2022)
16. Rombach, R., Blattmann, A., Lorenz, D., Esser, P., Ommer, B.: High-resolution image synthesis with latent diffusion models. In: Proceedings of the IEEE/CVF Conference on Computer Vision and Pattern Recognition. pp. 10684–10695 (2022)
17. Ronneberger, O., Fischer, P., Brox, T.: U-net: Convolutional networks for biomedical image segmentation. In: Medical Image Computing and Computer-Assisted Intervention–MICCAI 2015: 18th International Conference, Munich, Germany, October 5-9, 2015, Proceedings, Part III 18. pp. 234–241. Springer (2015)
18. Schlemper, J., Caballero, J., Hajnal, J.V., Price, A., Rueckert, D.: A deep cascade of convolutional neural networks for mr image reconstruction. In: Information Processing in Medical Imaging: 25th International Conference, IPMI 2017, Boone, NC, USA, June 25-30, 2017, Proceedings 25. pp. 647–658. Springer (2017)
19. Vaswani, A., Shazeer, N., Parmar, N., Uszkoreit, J., Jones, L., Gomez, A.N., Kaiser, Ł., Polosukhin, I.: Attention is all you need. Advances in neural information processing systems **30** (2017)
20. Wei, H., Li, Z., Wang, S., Li, R.: Undersampled multi-contrast mri reconstruction based on double-domain generative adversarial network. IEEE Journal of Biomedical and Health Informatics **26**(9), 4371–4377 (2022)
21. Xie, Y., Li, Q.: Measurement-conditioned denoising diffusion probabilistic model for under-sampled medical image reconstruction. In: Medical Image Computing and Computer Assisted Intervention–MICCAI 2022: 25th International Conference, Singapore, September 18–22, 2022, Proceedings, Part VI. pp. 655–664. Springer (2022)
22. Yu, C., Guan, Y., Ke, Z., Liang, D., Liu, Q.: Universal generative modeling in dual-domain for dynamic mr imaging. arXiv preprint arXiv:2212.07599 (2022)
23. Zbontar, J., Knoll, F., Sriram, A., Murrell, T., Huang, Z., Muckley, M.J., Defazio, A., Stern, R., Johnson, P., Bruno, M., et al.: fastmri: An open dataset and benchmarks for accelerated mri. arXiv preprint arXiv:1811.08839 (2018)
24. Zhao, J., Li, D., Kassam, Z., Howey, J., Chong, J., Chen, B., Li, S.: Tripartitegan: Synthesizing liver contrast-enhanced mri to improve tumor detection. Medical image analysis **63**, 101667 (2020)